Supplementary Information

Size-Dependent Reliability of Empirical Potentials for Global Optimization of Pt-Cu Bimetallic Clusters

Xiaomin Wu [a], Yousi Lin *[a], Miao He [b], Yuheng Chen [c] and Hua Shi [a]

[a] *School of Opto-Electronic and Communication Engineering, Xiamen University of Technology, Xiamen, China. E-mail: wuxiaomin@xmut.edu.cn, linyousi@xmut.edu.cn, shihua@xmut.edu.cn*
[b] *School of Electrical Engineering and Automation, Xiamen University of Technology, Xiamen, China. E-mail: hemiao@xmut.edu.cn*
[c] *Pen-Tung Sah Institute of Micro-Nano Science and Technology, Xiamen University, Xiamen, China. E-mail: hyc2537@163.com*

Table of Content

S1. Empirical-Potential Parameter Sets

The empirical-potential global searches in this work were carried out with the parameter sets summarized in Tables S1-S3. These tables are provided so that the comparison reported in the main text can be reproduced independently and so that the role of parameter choice can be examined separately from the role of the functional form.

Table S1. Gupta-potential parameters used in the global search.

Pair	A (eV)	ξ (eV)	p	q	r_0 (Å)
Pt-Pt	2.7747	0.2975	2.695	10.612	4.004
Cu-Cu	2.556	0.0894	1.224	10.96	2.278
Pt-Cu	2.665	0.1631	1.8162	10.7860	3.141

The values are taken from Ref. [21] of the main text.

Table S2. Sutton-Chen parameters used in the global search.

Pair	ξ (eV)	a (Å)	C	m	n
Pt-Pt	0.0097894	71.336	3.9163	11	7
Cu-Cu	0.0057921	84.843	3.6030	10	5
Pt-Cu	0.0075300	78.0895	3.75965	10.5	6

The values are taken from Ref. [23] of the main text.

Table S3. Finnis-Sinclair parameters used in the global search.

Pair	cutoff	c0	c1	c2	d	c	beta
Pt-Pt	3.80	1.24	-0.36	-0.04	4.00	1.83	1.8
Cu-Cu	3.50	1.24	-0.36	-0.04	3.70	1.83	1.8
Pt-Cu	3.65	1.24	-0.36	-0.04	3.85	1.83	1.8

The values are taken from Ref. [24] of the main text.

The parameter sets in Tables S1-S3 were applied without further refitting throughout the present benchmark. We emphasize that the assessment in the main text characterizes the behavior of each potential under the specific parameter set listed here.

S2. DFT Candidate Coverage Across Composition

To test whether the empirical-potential candidates map to the same part of the DFT landscape across composition, Table S4 compares Cu-rich, near-equiatomic, and Pt-rich cases rather than relying on a single composition. The key N = 23 result is that the DFT-lowest candidate changes with composition, indicating that different empirical potentials can locate DFT-competitive basins in different parts of Pt-Cu composition space.

The composition-resolved DFT energies in Figure S1 show two complementary trends. At N = 13, the three potentials are essentially degenerate at the off-equiatomic compositions Pt_3Cu_{10} and $Pt_{10}Cu_3$ in line with the strong icosahedral motif consensus reported in the main text; only at the near-equiatomic point Pt_6Cu_7 does the FS candidate become clearly distinguishable, lying 0.665 eV above the near-degenerate Gupta and SC candidates. At N = 23, by contrast, the DFT-lowest empirical potential rotates with composition: FS is lowest in the Cu-rich case (Pt_5Cu_{18}), SC is lowest at the near-equiatomic composition ($Pt_{11}Cu_{12}$), and Gupta is lowest in the Pt-rich case ($Pt_{18}Cu_5$). This composition-dependent rotation, summarized in Table S4, is the direct DFT-level evidence supporting the size- and composition-dependent reliability picture emphasized in the main text.

Table S4. Composition-dependent DFT-lowest empirical-potential candidate for the tested N = 23 cases.

Composition regime	Tested case	DFT-lowest candidate
Cu-rich	N = 23, Pt5Cu18	FS
Near-equiatomic	N = 23, Pt11Cu12	SC
Pt-rich	N = 23, Pt18Cu5	Gupta

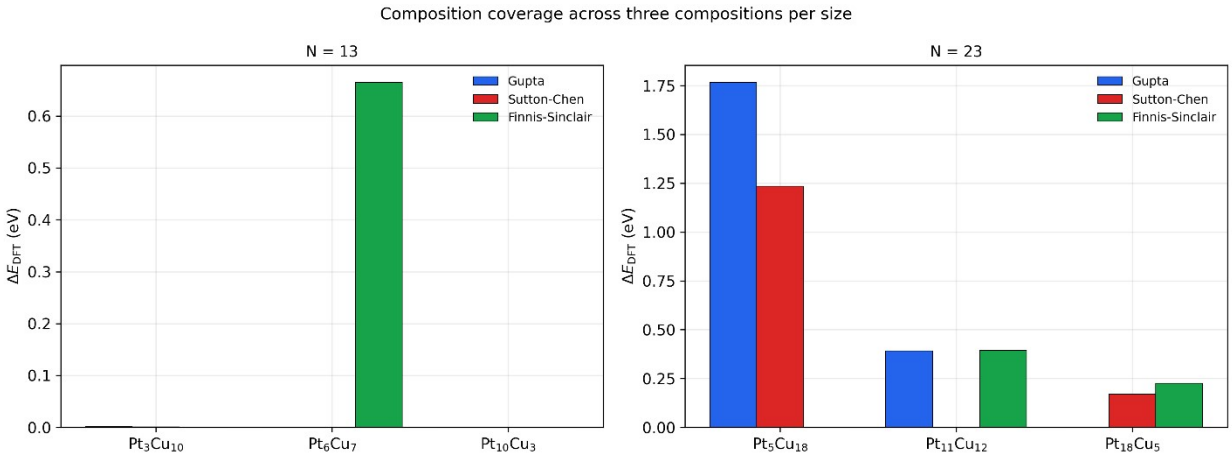

Figure S1. Composition-coverage comparison showing that the DFT-lowest empirical-potential candidate changes across the tested Cu-rich, near-equiatomic, and Pt-rich N = 23 cases.

S3. Structural Retention after DFT Relaxation

For the cluster sizes where full DFT ionic relaxation was carried out (N = 13 and N = 23), the structural response of each empirical-potential candidate is summarized in Table S5. The root-mean-square displacement (RMSD) between the EP-optimized geometry and the corresponding relaxed DFT geometry quantifies how strongly each candidate is reorganized when first-principles forces take over; the maximum residual force at the end of the relaxation verifies that all reported geometries are converged with respect to the force criterion stated in the main-text Methods section.

Table S5. EP-to-DFT structural retention for the tested Pt-Cu candidates at N = 13 and N = 23.

N	Composition	Potential	RMSD (Å)	Max residual force (eV/Å)
13	Pt_6Cu_7	Gupta	0.107	0.029
13	Pt_6Cu_7	SC	0.065	0.033
13	Pt_6Cu_7	FS	0.124	0.025
13	Pt_3Cu_{10}	Gupta	0.098	0.031
13	Pt_3Cu_{10}	SC	0.080	0.030
13	Pt_3Cu_{10}	FS	0.129	0.030
13	$Pt_{10}Cu_3$	Gupta	0.236	0.025
13	$Pt_{10}Cu_3$	SC	0.249	0.026
13	$Pt_{10}Cu_3$	FS	0.334	0.026
23	$Pt_{11}Cu_{12}$	Gupta	0.357	0.028
23	$Pt_{11}Cu_{12}$	SC	0.097	0.024
23	$Pt_{11}Cu_{12}$	FS	0.499	0.021
23	Pt_5Cu_{18}	Gupta	0.333	0.014
23	Pt_5Cu_{18}	SC	0.087	0.026
23	Pt_5Cu_{18}	FS	0.158	0.029
23	$Pt_{18}Cu_5$	Gupta	0.215	0.027
23	$Pt_{18}Cu_5$	SC	0.197	0.035
23	$Pt_{18}Cu_5$	FS	0.679	0.027

The values in Table S5 support the qualitative trends described in the main-text RMSD discussion: SC-derived candidates exhibit the smallest structural rearrangement upon DFT relaxation across the tested cases, FS-derived candidates undergo the largest reorganization

(most clearly at N = 23), and Gupta-derived candidates lie in between. The simultaneous convergence of the maximum residual force across all reported cases confirms that the RMSD differences reflect genuine structural retention rather than incomplete relaxation.

S4. Additional Structure-Origin Evidence for the N = 38 FS Basin

As shown in Table S6, the compact FS candidate at N = 38 is distinguished by a pronounced feature near 143° in the bonded-dihedral distribution. This feature is treated here as a structural signature of the FS-specific local packing pattern rather than, by itself, as evidence of energetic preference on the DFT landscape.

Table S6. Supplementary summary of the N = 38 bonded-dihedral enrichment near 143°.

Metric	FS candidate	Gupta reference
Dihedrals within 143° ± 5°	731 / 9869 (7.4%)	9 / 7248 (0.1%)
Dominant central-bond character	Pt-Pt 60.6%, Pt-Cu 36.4%, Cu-Cu 3.0%	No comparable enrichment at 143°

The contrast between Figures S2 and S3 makes the FS-specific nature of the 143° dihedral feature explicit. The FS distribution is continuous and broadly populated, with the 143° band carrying about 7% of the total dihedral count; the Gupta distribution is concentrated at a few discrete angles, with essentially no occupation of the 143° band. Combined with the central-bond breakdown in Table S6 (Pt-Pt 60.6%, Pt-Cu 36.4%, Cu-Cu 3.0% within the 143° window of the FS candidate), this confirms that the 143° feature is a fingerprint of an FS-specific compact, Pt-rich local packing pattern rather than a shared structural property at N = 38.

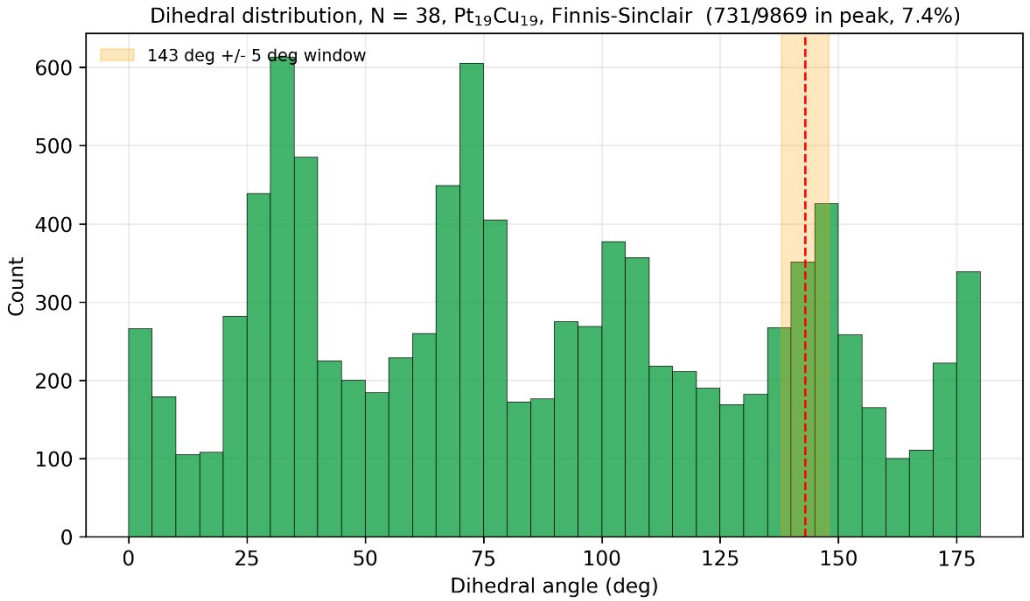

Figure S2. Dedicated bonded-dihedral analysis for the N = 38 FS candidate at Pt19Cu19, highlighting the supplementary 143° structural signature.

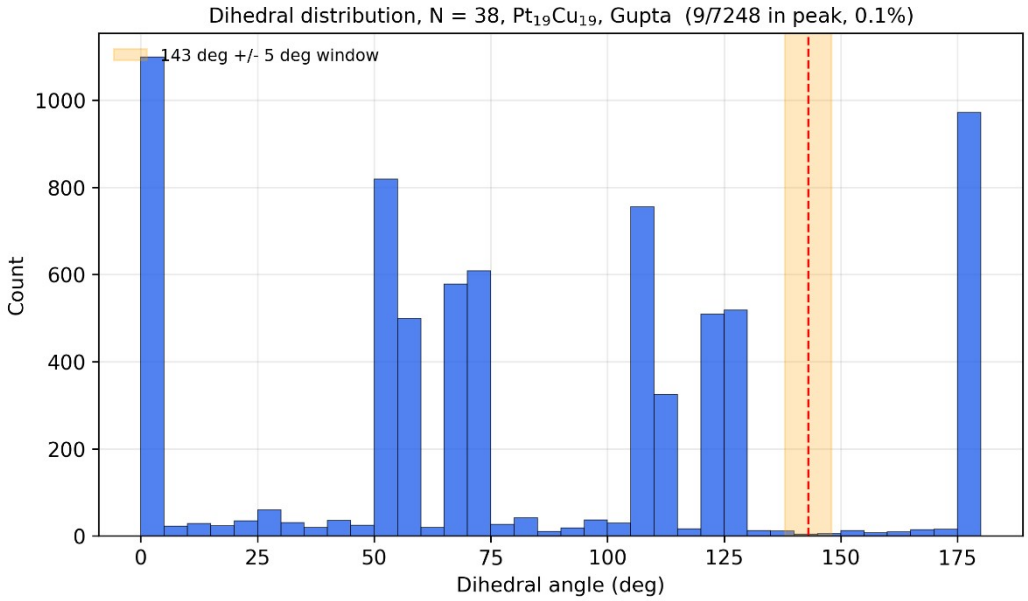

Figure S3. Gupta reference bonded-dihedral analysis for N = 38, shown for comparison with the FS-specific 143° enrichment.

S5. Single-point DFT energy comparison at Common Near-Equiatomic Compositions

Figure S4 visualizes the single-point DFT screening that underpins the DFT ranking discussed in the main text. At each size, the EP-optimized global minimum at the common near-equiatomic composition is re-evaluated by DFT, and the three candidates are reported relative to the lowest-energy structure. At N = 13, the Gupta and SC candidates are degenerate within numerical precision and the FS candidate lies 0.665 eV higher. At N = 23, the SC candidate is lowest, while the Gupta and FS candidates are higher by 0.392 and 0.393 eV, respectively. At N = 38, the SC candidate remains lowest, the Gupta candidate is 1.038 eV higher, and the FS compact 143°-signature motif is 2.895 eV higher. The ordering changes with cluster size and is not predictable from the EP-internal energetic preferences alone, supporting the main-text conclusion that descriptor-level rankings and DFT energetic competitiveness do not collapse into a single ranking.

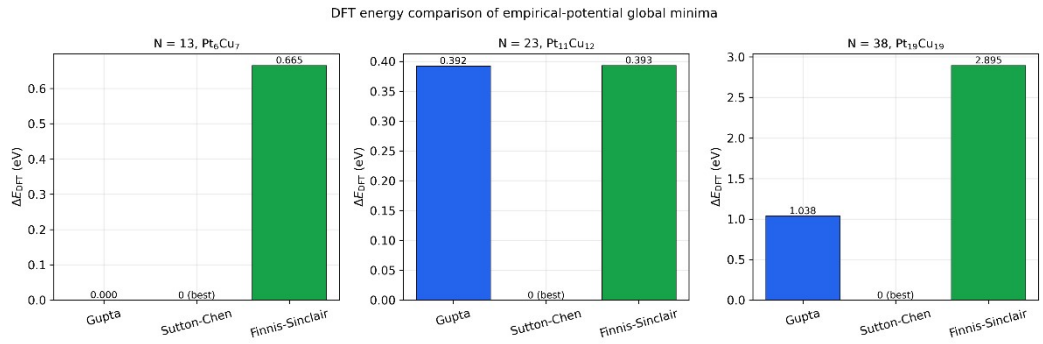

Figure S4. DFT energy comparison of the EP-optimized global minimum structures at the common near-equiatomic compositions, Pt_6Cu_7 for N = 13, $Pt_{11}Cu_{12}$ for N = 23, and $Pt_{19}Cu_{19}$ for N = 38. For each size, ΔE_DFT is referenced to the lowest-energy candidate among the three potentials (labeled "0 (best)").